

PHASE-DEPENDENT SPECTROSCOPY OF MIRA VARIABLE STARS

MICHAEL W. CASTELAZ^{1,2} AND DONALD G. LUTTERMOSER

Department of Physics, East Tennessee State University, Box 70652, Johnson City, TN 37614, and Southeastern Association for Research in Astronomy;
castelam@etsu.edu, lutter@etsu.edu

DANIEL B. CATON

Department of Physics and Astronomy, Dark Sky Observatory, Appalachian State University, Boone, NC 28608; catonb@appstate.edu

AND

ROBERT A. PIONTEK^{1,3}

University of Maryland, Department of Astronomy, College Park, MD 20742; rpiontek@ra.astro.lsa.umich.edu

Received 1998 December 14; accepted 2000 July 24

ABSTRACT

Spectroscopic measurements of Mira variable stars as a function of phase probe the stellar atmospheres and underlying pulsation mechanisms. For example, measuring variations in TiO, VO, and ZrO with phase can be used to help determine whether these molecular species are produced in an extended region above the layers where Balmer line emission occurs or below this *shocked* region. Using the same methods, the Balmer line *increment*, where the strongest Balmer line at phase zero is H δ and not H α , can be measured and explanations tested, along with another peculiarity, the absence of the H ϵ line in the spectra of Mira variables when the other Balmer lines are strong. We present new spectra covering the spectral range from 6200 to 9000 Å of 20 Mira variables. A relationship between variations in the Ca II IR triplet and H α as a function of phase support the hypothesis that H ϵ 's observational characteristics result from an interaction of H ϵ photons with the Ca II H line. New periods and epochs of variability are also presented for each star.

Key words: Miras — techniques: spectroscopic

1. INTRODUCTION

Mira-type variable stars are large, cool stars whose visual light variations exceed 2.5 mag over periods from 150 to ~500 days. The light curves of Mira variables depend on the surface temperature, radius, and opacity, all of which vary as the star pulsates. These pulsations extend the atmosphere beyond that of the hydrostatic equilibrium configuration and enhance mass loss in these stars (Maciel 1977; Willson & Hill 1979; Bertschinger & Chevalier 1985; Bowen 1988; Fleischer et al. 1992, 1995). As a result, Mira variables are an important component in seeding the interstellar medium with C, N, and O.

These stars are located on the asymptotic giant branch, a transitional phase in stellar evolution. Photometric and spectroscopic measurements of their light curves provide a means to probe the stellar atmospheres and underlying pulsation mechanisms occurring during this stellar phase. In the near infrared, the spectra of Mira stars are dominated by the TiO γ system, the VO γ system, and ZrO (Wing 1967). The TiO features are thought to be produced in a layer somewhat far from the photosphere (Gillet 1988). Haniff et al. (1992) present optical aperture synthetic images of the photosphere of *o* Ceti at 6500 Å, 7007 Å, and within a TiO band head at 7099 Å, with the star phase ~0.94. They find asymmetry in the images, with the TiO image 1½ times larger than the photospheric images. Also, narrowband speckle interferometric measurements taken in the TiO 7120 Å band head and outside at 7400 Å by Labeyrie et al.

(1977) show that the diameters of R Leo and *o* Ceti are twice as large in the TiO feature than outside of it. This demonstrates that a model atmosphere, based on the spectra observed over a TiO bandpass, provides parameters such as T_{eff} and $\log g$ in an atmospheric layer far from the photosphere.

Joy (1926) presents a comprehensive, phase-dependent, spectroscopic (35 Å mm⁻¹) study of a prototype Mira variable, *o* Ceti. Analyzing 131 spectra taken over a 10 yr period, Joy describes several important characteristics. Briefly, the spectra of *o* Ceti show that TiO bands vary with magnitude, hydrogen emission lines appear with greatest intensity at or shortly after maximum visual brightness (phase zero), ionized iron emission lines are observed at maximum, and the temperature is estimated to vary from 1800 to 2300 K. Absorption lines (including iron, vanadium, chromium, manganese, calcium, and magnesium) were used to measure a variation in radial velocity. The maximum positive velocity occurs at phase zero, and the greatest blue-shift occurs at minimum light. Later, Joy (1954) took 88 spectrograms of *o* Ceti at a higher spectral resolution (typically 10.3 Å mm⁻¹) and confirmed that maximum velocity of recession occurs soon after visual maximum. He attributed these results to a pulsational mechanism and suggested the possibility of shocks.

Perhaps one of the most interesting characteristics of Mira spectra is the strong hydrogen Balmer line emission that is seen throughout much of the pulsation cycle. As Pickering (1887) first noticed in spectra of *o* Ceti and as was later described in detail by Joy (1926, 1947, 1954), the hydrogen Balmer emission-line flux in relation to the nearby *photospheric* (i.e., pseudocontinuum) flux is unique in the oxygen-rich (M-type) Mira spectra: Balmer H α emission is typically weaker than H β , which, in turn, is weaker than H γ near peak visual brightness. H δ is seen as the

¹ Visiting Astronomer, Dark Sky Observatory, Appalachian State University.

² Also at Pisgah Astronomical Research Institute.

³ Participant, summer 1998 Southeastern Association for Research in Astronomy, Research Experience for Undergraduates Program, sponsored by the National Science Foundation.

strongest Balmer emission line at phase zero. Lines higher in the series (i.e., toward shorter wavelengths) are weaker. This *Balmer increment* (i.e., $F_{H\alpha} < F_{H\beta} < F_{H\gamma} < F_{H\delta}$) is just opposite of what would be expected. $H\alpha$, having the largest oscillator strength, should be stronger than $H\beta$, and the higher order Balmer lines should be weaker down the line (i.e., one should see a Balmer line *decrement*), assuming these lines all form in the same region of the atmosphere (i.e., similar T and P). Meanwhile, in S-type and carbon star (N-type) Mira variables, the strength of the Balmer lines approximately follow their expected respective oscillator strengths (Merrill 1940, p. 44).

For years, this Balmer line increment in the M-type Mira variables has been attributed to TiO absorption, which hides $H\alpha$, $H\beta$, and $H\gamma$ fluxes (Merrill 1940; Joy 1947; Gillet 1988), although there is some debate of the effect that this or other molecular absorption has on the $H\alpha$ line (Gillet, Maurice, & Baade 1983; Gillet et al. 1985). Recently, another explanation has been given for this Balmer increment: non-LTE (NLTE) radiative transfer calculations of hydrodynamic models representative of Mira variables (Bowen 1988) suggest that the Balmer increment results from radiative transfer effects in the hydrogen lines themselves when formed in a shocked atmosphere (Luttermoser & Bowen 1992; Luttermoser, Bowen, & Willson 2000). In these calculations, $H\alpha$, having the highest optical depth, forms just in front of the innermost shock. $H\beta$ then forms a little deeper as a result of its lower optical depth, and $H\gamma$ deeper still. The optical depth of $H\delta$ causes it to arise from the hottest part of the shock, and hence it extends higher above the continuum than the longward Balmer lines. Then, as one goes to higher order lines in the series, the opacity in these lines is not high enough in the shock for these lines to form there—we see through the shock at these transitions. As such, this increment may be giving us information on the shock thickness for Mira variables and may indicate that the shock structure of the S-type and N-type

Mira variables is fundamentally different from that of the M-type Mira variables. Future NLTE radiative hydrodynamic models of Mira variables with different C/O ratios are needed to see if this is the case. It is likely that a combination of both processes (i.e., TiO absorption and NLTE radiative transfer effects) are responsible for this Balmer line increment.

Another striking feature is the weakness (and often absence) of the He line (3970.074 Å) in the Balmer series near maximum visual brightness (see Gillet 1988). Merrill (1940) noted this and suggested this weakness was a result of the interaction between the He transition and the Ca II H line (3968.470 Å) wing. Castelaz & Luttermoser (1997, hereafter CL97) concur with this suggestion. Briefly, the He photons may be scattered by the Ca II H line out to IR wavelengths via the 8662 Å line. Of the three lines in the Ca II IR triplet, the 8498 and 8542 Å lines share the same upper level of the Ca II K line, whereas the 8662 Å line shares the same upper level as the Ca II H line. As such, if He photons are being scattered by Ca II H, the $\lambda 8662$ will show variations independent of the other two Ca II IR triplet lines and can be tested by monitoring the strength of the absorption of this 8662 Å line as compared with the 8498 and 8542 Å lines as a function of phase in the Mira stars.

Ca II IR triplet observations of Mira variables have been carried out by Contadakis & Solf (1981) and Gillet et al. (1985). Unfortunately, Contadakis & Solf (1981) only made one observation of the 8662 Å line in their monitoring program of S-type Mira variables. They observed $\lambda 8498$ and $\lambda 8542$ in emission in many of the stars in their sample near phase zero and as absorption lines at other phases, so we cannot use their data to test our proposed hypothesis. Gillet et al. (1985) observed P Cygni profiles in the Ca II IR triplet lines near phase zero in the hot Mira variable S Car. Once again, only one spectrum of the 8662 Å line was obtained in their sample of Ca II spectra. CL97 present a set of phase-dependent spectra taken especially to address this

TABLE 1
MIRA VARIABLES

Star	R.A. (J2000.0)	Decl. (J2000.0)	Spectral Type	V_{\max}	V_{\min}	Period (days)	Epoch (2,450,000+)
T Cas	00 23 14	+55 47 34	M7e	7.3	12.4	433.67	733
W And	02 17 33	+44 18 20	M7: p	6.7	14.5	386.08	638
σ Cet	02 19 21	−02 58 28	M7 IIIe	2.0	10.1	321.58	496
R Tri	02 37 02	+34 15 52	M4 IIIe	6.2	11.7	265.48	568
R Tau	04 28 18	+10 09 48	M6e	8.6	14.2	313.34	1069
U Ori	05 55 49	+20 10 31	M8 III	6.3	12.0	367.00	1120
R Leo	09 47 33	+11 25 45	M8 IIIe	5.8	10.0	309.13	1060
V CVn	13 19 27	+45 31 38	M6 IIIa	6.8	8.8	188.74	849
R CVn	13 48 57	+39 32 34	M6 IIIe	7.7	11.9	328.00	793
V Boo	14 29 45	+38 51 41	M6e	7.0	11.3	258.95	820
R Boo	14 32 12	+26 44 11	M4e	6.7	12.8	224.39	559
S CrB	15 21 24	+31 22 04	M7e	6.5	14.1	367.23	785
R Ser	15 50 42	+15 08 03	M7 IIIe	5.7	14.4	357.74	860
W Her	16 35 12	+37 20 42	M3e	8.3	13.5	280.15	915
RS Her	17 21 42	+22 55 16	M5e	7.9	12.5	217.68	869
T Her	18 09 06	+31 01 16	M4e	8.0	12.8	163.70	897
W Lyr	18 14 56	+36 40 13	M4.5e	7.9	12.2	195.50	411
χ Cyg	19 50 33	+32 54 53	MS	5.2	13.4	419.97	736
T Cep	21 09 32	+68 29 28	M7 IIIe	6.0	10.3	398.00	548
W Peg	23 19 51	+26 16 44	M7e	8.2	12.7	330.00	711

NOTE.—Units of right ascension are hours, minutes, and seconds, and units of declination are degrees, arcminutes, and arcseconds.

problem of He photon scattering by Ca II. Spectra of seven Mira variables were taken at different phases and suggest a possible anticorrelation between H α emission and Ca II λ 8662 absorption. Assuming that the He I line-strength variations are in phase with H α , then the apparent anticorrelation between the strength of the H α emission line and the strength of the Ca II 8662 Å line suggests that a *fluorescence* is taking place in the Ca II 8662 Å line with He I serving as the pump through the Ca II H line. In this paper we present phase-dependent spectra of 20 Mira variables to

further explore the anticorrelation of Ca II λ 8662 absorption with H α emission.

2. OBSERVATIONS

The 20 stars for which spectra are presented, their equatorial coordinates, mean spectral types, and visual maxima and minima taken from the SIMBAD database are given in Table 1. Also listed in Table 1 are new ephemerides of these Mira stars. We calculated the ephemerides from AAVSO light curves measured within the previous 8 yr. The curves

TABLE 2
LOG OF OBSERVATIONS

Star	Observation Date (UT)	Observation JD (2,450,000+)	Visible Phase	<i>V</i>	Integration Time (s)	Telescope
T Cas	1997 Nov 1	753.5	0.04	8.0	120	SARA
	1998 Nov 15	1132.5	0.92	10.2	300	SARA
W And	1997 Nov 2	754.5	0.30	13.4	900	SARA
<i>o</i> Cet	1997 Nov 1	753.5	0.80	7.1	60	SARA
R Tri	1997 Feb 15	494.5	0.73	10.0	1800	SARA
	1997 Mar 13	520.5	0.83	8.6	600	DSO
	1997 Nov 1	753.5	0.70	10.3	180	SARA
R Tau	1997 Feb 15	494.5	0.16	11.7	360	SARA
	1997 Nov 1	753.5	0.99	8.9	180	SARA
	1998 Nov 14	1131.5	0.20	11.2	300	SARA
U Ori	1997 Feb 14	493.5	0.30	10.7	600	SARA
	1997 Nov 1	753.5	0.01	6.6	60	SARA
	1998 Feb 15	859.5	0.29	10.5	600	SARA
	1998 Nov 14	1131.5	0.03	6.4	300	SARA
R Leo	1997 Feb 14	493.5	0.16	8.5	600	SARA
	1997 Mar 13	520.5	0.25	9.2	600	DSO
	1997 May 28	596.5	0.49	10.0	600	SARA
	1998 Feb 15	859.5	0.34	9.8	300	SARA
	1998 Mar 28	900.5	0.48	10.0	300	DSO
	1998 May 24	957.5	0.66	9.2	60	SARA
	1998 Nov 14	1131.5	0.23	8.8	300	SARA
	1997 Feb 14	493.5	0.12	7.0	240	SARA
V CVn	1997 Mar 13	520.5	0.27	7.9	600	DSO
	1997 May 25	593.5	0.65	8.8	600	SARA
	1998 Feb 15	859.5	0.06	7.1	600	SARA
	1998 May 23	956.5	0.57	8.8	300	SARA
R CVn	1997 Feb 15	494.5	0.09	8.5	600	SARA
	1997 Mar 13	520.5	0.17	9.5	600	DSO
	1997 May 26	583.5	0.39	11.3	1800	SARA
	1998 Feb 15	859.5	0.20	9.9	600	SARA
V Boo	1998 May 23	956.5	0.50	11.9	300	SARA
	1997 Feb 15	494.5	0.12	8.3	600	SARA
	1997 May 26	595.5	0.51	11.3	600	SARA
R Boo	1998 May 24	957.5	0.53	8.5	240	SARA
	1997 May 25	583.5	0.11	8.2	600	SARA
	1998 May 24	957.5	0.47	13.5	600	SARA
S CrB	1997 May 25	593.5	0.48	13.6	1800	SARA
R Ser	1998 May 24	957.5	0.26	6.5	1200	SARA
	1997 May 25	593.5	0.26	6.5	1200	SARA
W Her	1998 May 23	956.5	0.27	6.9	300	SARA
	1997 May 26	594.5	0.86	9.8	1200	SARA
RS Her	1998 May 24	957.5	0.15	11.4	900	SARA
	1997 May 28	596.5	0.75	11.0	1800	SARA
T Her	1998 May 23	956.5	0.40	12.3	420	SARA
	1997 May 26	594.5	0.15	10.3	1200	SARA
W Lyr	1998 May 24	957.5	0.37	12.4	1200	SARA
	1997 May 26	594.5	0.94	8.9	900	SARA
χ Cyg	1997 May 26	594.5	0.66	11.8	300	SARA
	1997 Nov 1	753.5	0.04	7.6	60	SARA
T Cep	1998 Jul 19	1013.5	0.66	11.3	120	SARA
	1997 Nov 2	754.5	0.52	10.2	300	SARA
W Peg	1997 Nov 1	753.5	0.13	9.0	600	SARA

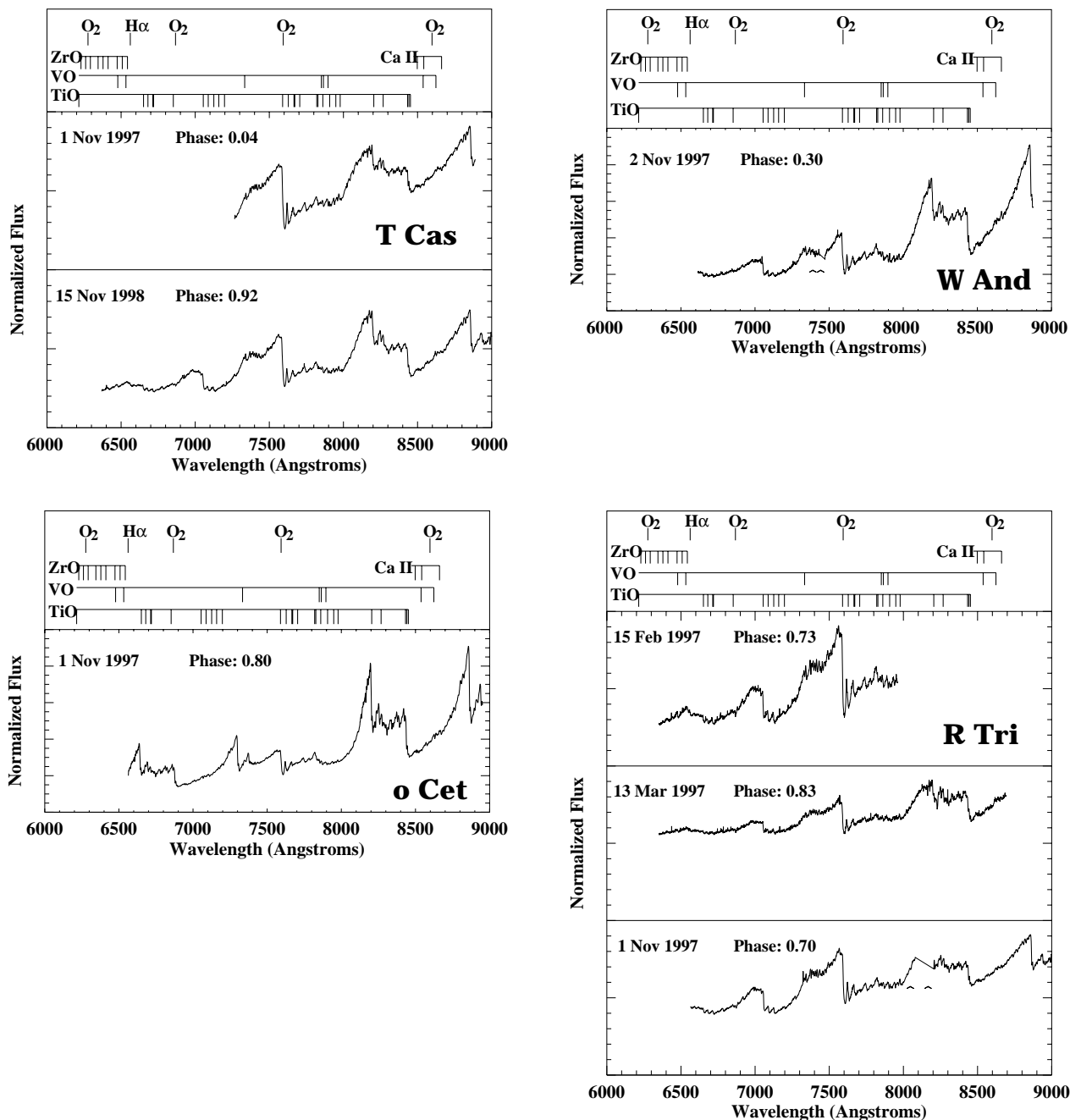


FIG. 1.—Spectra of the 20 Mira variables. The name of the star, date, and phase are given on each spectrum. The flux is normalized to 1. Above each set of spectra are markers for the major spectral features, as well as terrestrial oxygen. $H\alpha$ is weak or not seen in most of the spectra. Markers enclose regions of individual spectra where no data were taken. Spikes due to cosmic-ray hits in several spectra have not been removed.

were fitted with a linear combination of sine and cosine functions from which a new period and Julian date at phase zero were determined for each star.

Spectra of Mira variable stars were taken between 1997 February and 1998 November using a low-resolution spectrograph. Since we are interested in only monitoring absorption- and emission-line strengths for this program, low-resolution spectra are all that is required. The spectrograph was used at both the Southeastern Association for Research in Astronomy (SARA) 0.9 m telescope at Kitt Peak, and Appalachian State University's Dark Sky Observatory (DSO) 0.45 m telescope located near Boone, North Carolina. A converter lens was used at both sites to convert

the respective telescope f-ratios to about $f/11$ for the spectrograph.

The spectrograph was configured with a 600 groove mm^{-1} grating. The slit width was 100 μm . At the SARA 0.9 m telescope, the slit width was 3", and at the DSO 0.45 m telescope the slit width was 4". At both sites, the slit was parallel to the hour angle. A cooled 768 \times 512 CCD camera with 9 μm square pixels was used to record the spectra. The linear dispersion was 1.08 \AA pixel $^{-1}$, covering 768 pixels or 829 \AA on the CCD. The spectral resolution was measured to be 2.4 \AA . By rotating the grating up to four times per star, spectra were taken from about 6200 to 9000 \AA and included $H\alpha$, TiO, VO, and the Ca II infrared triplet lines. Integration

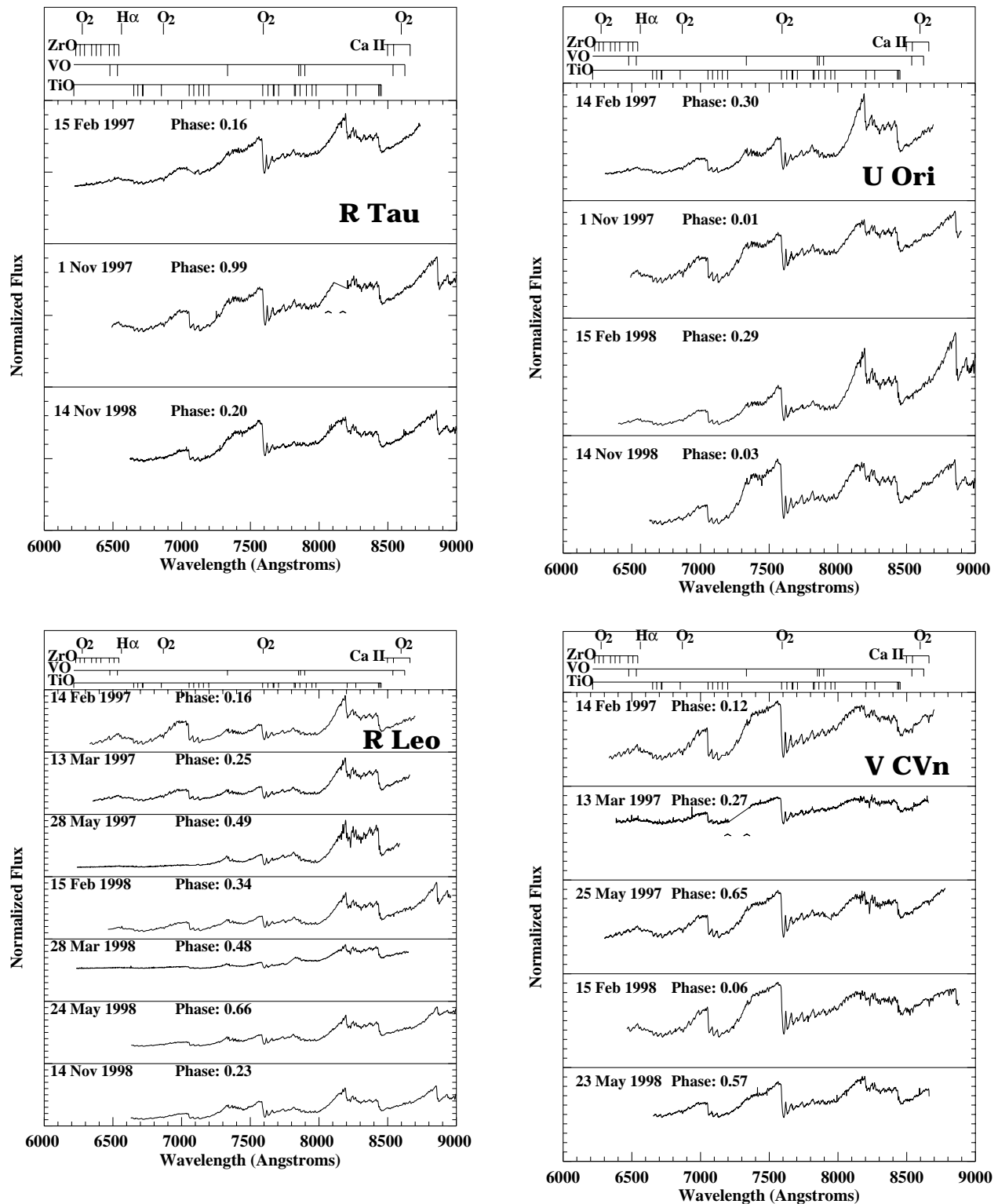


FIG. 1.—Continued

times were adjusted to achieve a signal-to-noise ratio greater than 100 for most spectra, except for the 1997 May spectra of W Her, T Her, and W Lyr, and the 1998 May spectrum of T Her.

Table 2 gives the log of observations for each star, which includes dates of observation, phase of the variable, approximate visual magnitude, integration time, and observing site. The phases listed in Table 2 were determined from the ephemerides given in Table 1 and refer to the visual phases,

with phase zero corresponding to maximum visual brightness. The visual magnitudes have been obtained from curve fits to the light curves from the AAVSO database. The method of phase determination used in this paper is not the standard method used by AAVSO. We used the AAVSO light curves observed at the same time as our observations to determine the phases. The AAVSO standard method to derive official phases dates of maximum and minimum may give different phases.

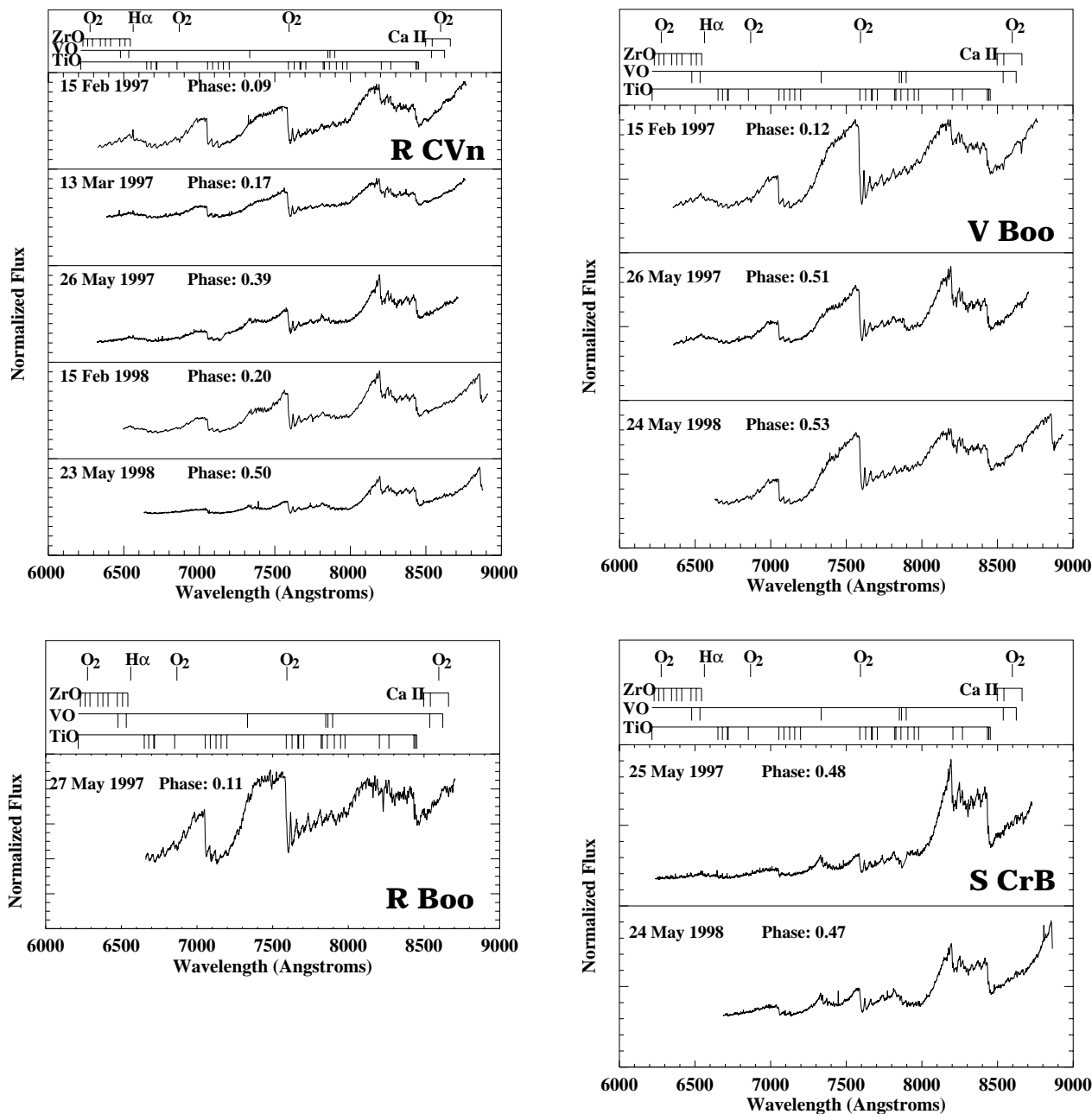


FIG. 1.—Continued

Dark frames and flat frames were taken for flat-fielding purposes. Spectra of neon lamp emission were taken simultaneously with the stellar spectra and used for wavelength calibration. We flat-fielded the images and extracted the spectra using MIRA software. The extracted spectra were wavelength-calibrated using the spectrum of neon superposed on the CCD frame with the stellar spectrum (Crowe, Heaton, & Castelaz 1996).

3. RESULTS

The spectra for the Mira variable stars are shown in Figure 1. The wavelengths of TiO, VO, ZrO, the Ca II IR triplet, H α , and terrestrial oxygen are marked above each set of spectra. Their wavelengths were identified in CL97. The ZrO and VO absorption overlap at 6574 and 6578 Å, and VO and TiO absorb at 7865 and 7861 Å, respectively. Because of the low dispersion of our spectra, these features

are blended. The appearance of a relatively narrow feature near 8230 Å is seen in some of the spectra—an \bar{o} Cet spectrum taken 1997 November 1 (phase 0.80), and spectra taken 1997 May 26–28 of R Leo (0.49), V CVn (0.65), R Boo (0.11), R Ser (0.26), RS Her (0.75), and W Lyr (0.94). This feature is due to terrestrial H $_2$ O at 8227 Å (Turnshek et al. 1985) and is an effective measure of the relative humidity in the air.

3.1. Radiative Transfer in the Ca II Ion

The transfer of radiation in the Ca II ion is very complicated. Besides He photons affecting the level populations of the $3d\ ^2P_{1/2}$ state through the Ca II H line, the hydrogen Ly α line lies just shortward of the Ca II ionization edge of the $3d\ ^2D_{3/2}$ (at 1218.1 Å) and the $3d\ ^2D_{5/2}$ (at 1219.0 Å) states. These two states are the lower levels of the Ca II IR triplet lines and are metastable. If Ly α is a strong emission

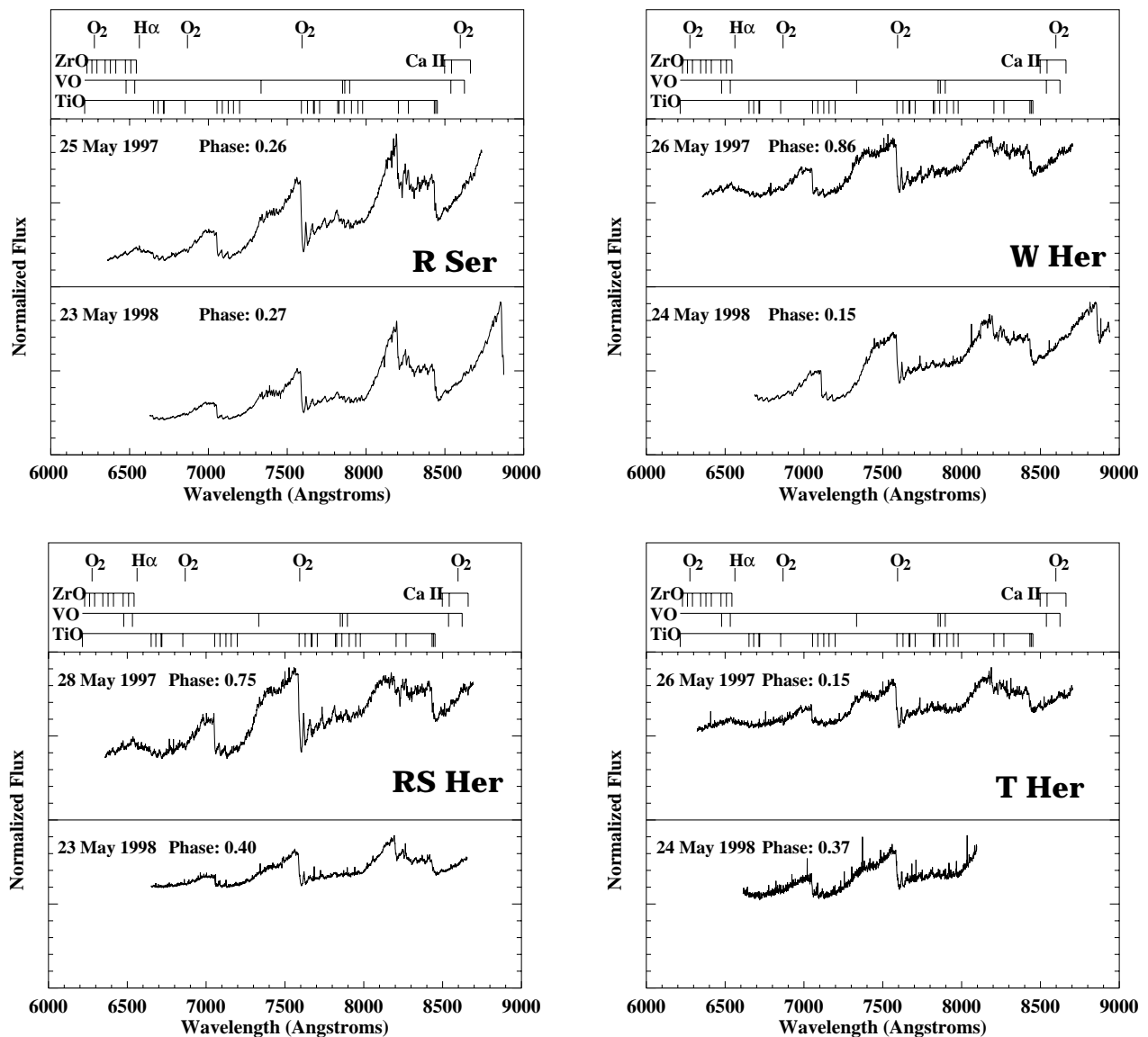


FIG. 1.—Continued

feature, and the Ca II 2D continuous opacity forms in a region of the atmosphere where the Ly α line is not yet in detailed balance, then Ly α photons may influence the Ca II IR triplet lines as well. Note that no observations have yet been made in the far-UV for Mira variables.

The line center of Ly α lies 2.4 Å shortward of the $^2D_{3/2}$ ionization edge and 3.3 Å shortward of the $^2D_{5/2}$ edge, so much of the Ly α emission profile can ionize Ca II out of the metastable state. The lower level of the Ca II 8662 Å line transition is the $^2D_{3/2}$ state, whose ionization edge lies slightly closer to Ly α than the $^2D_{5/2}$ edge. The following question arises: Will Ly α photons affect the level densities of the two $3d\ ^2D$ states differently? To answer this question, we ran a few atmospheric models with an arbitrarily located 10,000 K shock through the LTE stellar atmosphere code ATLAS (Kurucz 1970; Brown et al. 1989). Although it is likely that NLTE effects will dominate the level and ion densities in the atomic and molecular species (Luttermoser & Bowen 1992; Luttermoser, Bowen, & Willson 2000), these LTE runs are performed to merely determine the variation of the Ca II 2D continuous opacity across the Ly α profile. It also should be pointed out that in regions of the

atmosphere where LTE no longer applies, the assumptions of radiative and hydrostatic equilibria are no longer valid in these pulsating giant stars either. In fact, a Mira star has numerous shocks propagating through its atmosphere at any given time, as has been shown by Bowen (1988) and more recently by Höfner et al. (1998) and Loidl et al. (1999). Willson (2000) gives a very detailed review of all the dynamic modeling that has been performed on these pulsating stars and discusses the problems of carrying out NLTE radiative transfer in such a dynamic atmosphere.

We sampled atmospheric depths in front of the shock, in the shock, behind the shock, and deep in the photosphere where the continuum reaches optical depth unity in this region of the spectrum. We found that the continuous opacity from the Ca II $3d\ ^2D$ ionization remained constant (from both J sublevels) to within 0.15% from the location of the edges through 1210 Å, which should include most of the Ly α emission profile. The fact that the continuous opacity from Ca II remains constant across the Ly α profile indicates that Ly α will not preferentially affect the number density in the $^2D_{3/2}$ level as compared with the $^2D_{5/2}$ level—photoionizations of Ca II due to Ly α photons will affect the

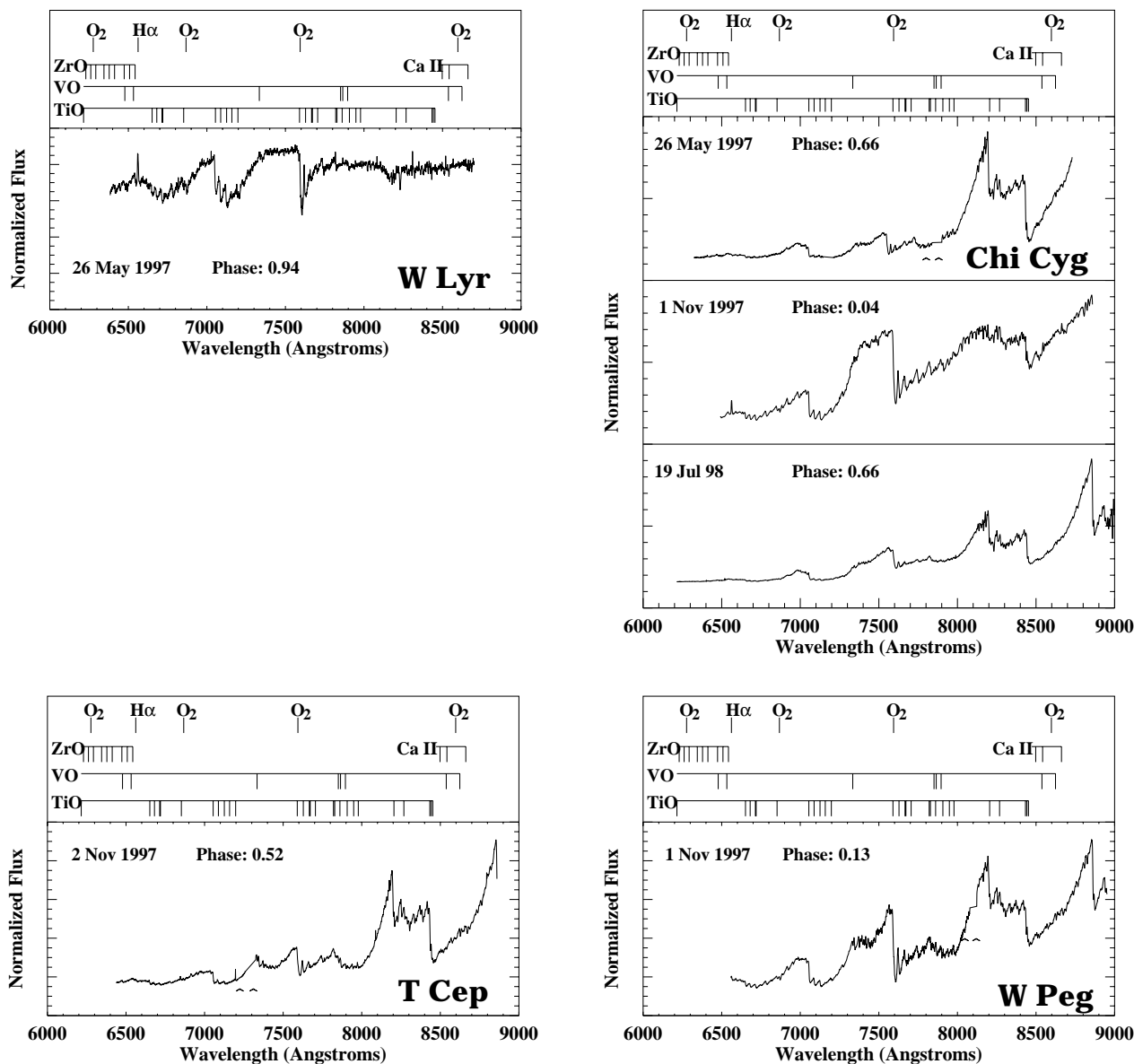


FIG. 1.—Continued

strengths of three Ca II IR lines in a similar fashion. Therefore, any variation in the 8662 Å line that is not seen in the other lines must result from some process other than Ly α photoionizations.

3.2. The H α Emission Line and Ca II IR Triplet

We are interested in the strength of the Ca II IR triplet compared with the strength of H α as a function of phase, since we are assuming that variations in H ϵ will mimic variations in H α . The Ca II IR triplet lines are not strong, as expected for stars later than M0 (Zhou 1991). A total of 27 spectra of 15 stars in our sample span the wavelength range from H α through the Ca II IR triplet. The remaining spectra are missing either the H α or the Ca II IR triplet regions of the spectrum because the spectrograph grating was not rotated sufficiently during observation to cover those parts of the spectrum.

The observations that show obvious H α emission features include U Ori (phase 0.29), R Leo (0.34), V CVn (0.12),

R CVn (0.09 and 0.17), R Ser (0.26), W Lyr (0.94), and χ Cyg (0.04). At the same phases, the Ca II λ 8662 is seen in emission in R Leo, R Ser, W Lyr, and χ Cyg, whereas the 8498 Å and 8542 Å lines stay in absorption or are not apparent. Ca II λ 8662 is not seen in emission in any other spectra that we took, only in those that show H α emission. The Ca II IR triplet can be seen in absorption in the remaining 23 spectra (although in some cases weakly), except for U Ori (phase 0.01), S CrB (0.48), W Her (0.86), and T Her (0.15), which do not appear to have any type of Ca II IR triplet features.

At this point, we call attention to three of the hydrogen Paschen lines that lie close to each Ca II IR triplet line: λ 8502.4 (4.4 Å redward from the Ca II 8498.0 Å line), λ 8545.3 (2.8 Å redward of the Ca II 8542.1 Å line), and λ 8665.0 (2.8 Å from the Ca II 8662.1 Å line), the Pa13, Pa12, and Pa10 lines, respectively. It has been shown by Gillet et al. (1985) that even though the Pa δ line is in emission in the spectrum of the Mira variable S Car, the higher order Paschen lines near the Ca II IR triplet are seen neither in absorption nor in

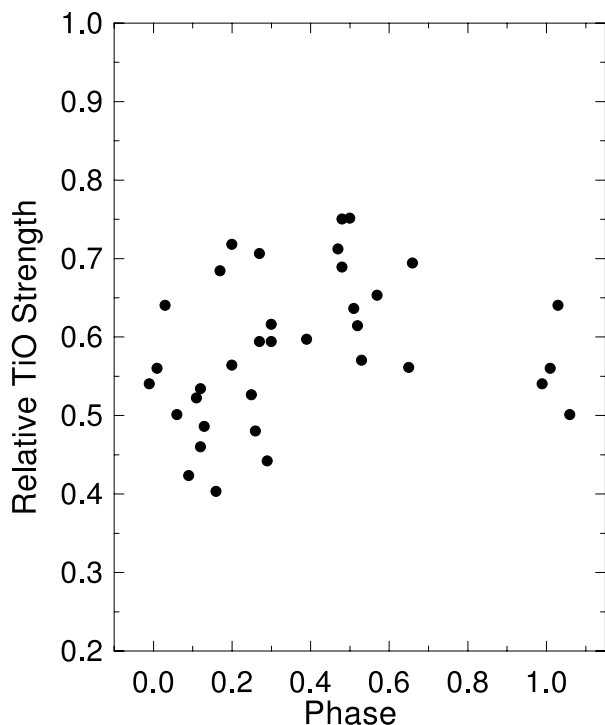


FIG. 2.—Integrated flux ratio of the 7060–7110 Å wavelength band (A) to that of the 6995–7045 Å band (B) plotted as a function of phase. Band A contains TiO opacity whereas band B is free of TiO, VO, and ZrO band heads. This plot contains only data from the M6, M7, and M8 spectral type Mira variables. No apparent trends are seen in the data, which indicates that variations in the $H\alpha$ flux result primarily from intrinsic flux variations in $H\alpha$ and not from varying overlying TiO absorption.

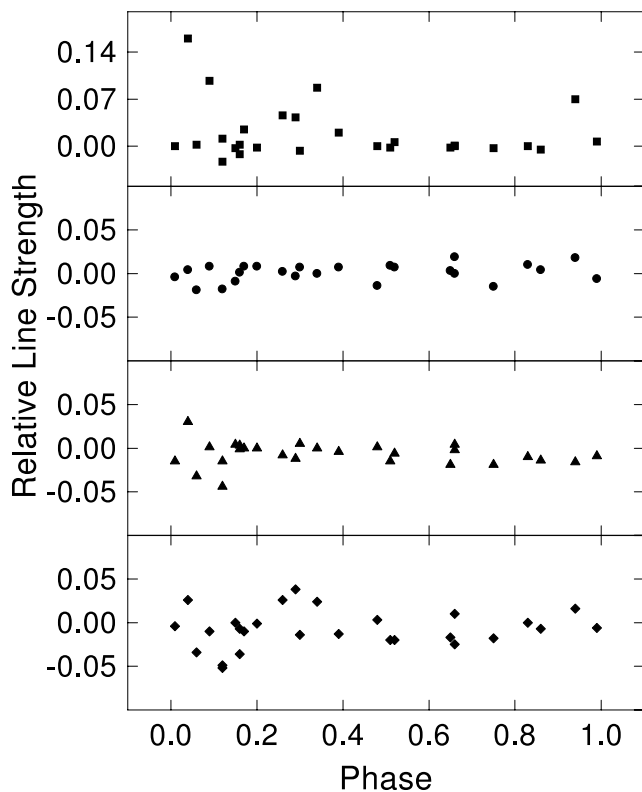


FIG. 3.—Relative line strengths of $H\alpha$ (squares) and Ca II lines at 8498 Å (circles), 8542 Å (triangles), and 8662 Å (diamonds) as a function of light variation phase. Variation in the Ca II lines at 8498 and 8542 Å mimic each other, whereas the Ca II line at 8662 Å does not follow the same trend. The uncertainty of the measurements is ± 0.007 .

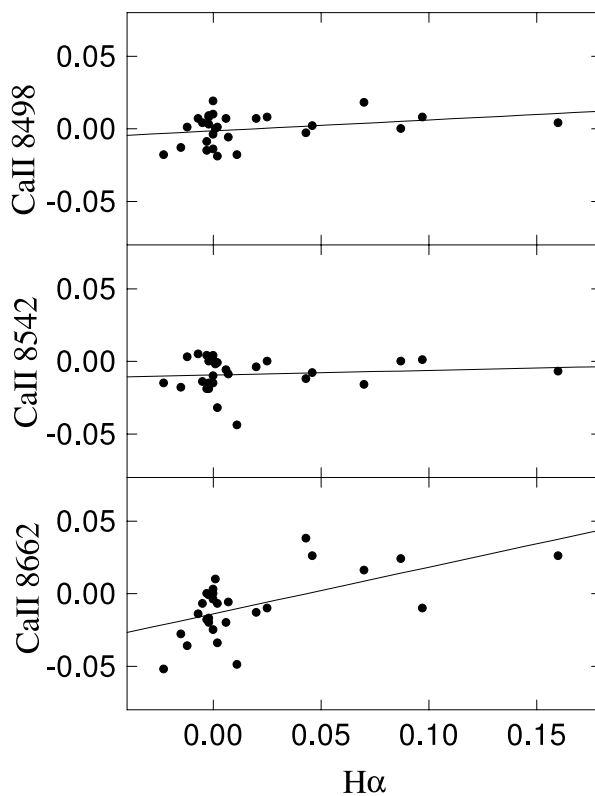


FIG. 4.—Relative line strengths of Ca II λ 8498, λ 8542, and λ 8662 vs. the relative line strength of $H\alpha$. The data of each plot are linearly fitted, and the results of the fits are drawn in the plots. Only the Ca II λ 8662 vs. $H\alpha$ plot shows a significant slope, which implies a correlation between the occurrence of the two features.

emission, analogous to the Balmer lines. As such, it is unlikely that these higher order Paschen lines are affecting the Ca II lines in our spectra.

3.3. The TiO Bands and $H\alpha$ Emission

In addition to the Ca II IR triplet, we are interested in comparing the TiO γ system's molecular features with $H\alpha$ emission as a function of phase. A qualitative comparison of $H\alpha$ emission with the molecular features can be made for U Ori, R Leo, R CVn, R Ser, W Lyr, and χ Cyg stars with phase-dependent spectra that also show the $H\alpha$ emission line in at least one spectrum. Weak $H\alpha$ emission is seen in U Ori at phase 0.29 on 1998 February 15. However, on the previous pulsation cycle, $H\alpha$ emission is not obvious at either phases 0.30 or 0.01, although there may be some very weak emission. Stronger $H\alpha$ emission is seen in R Leo (phase 0.34), R CVn (0.09, 0.17, and 0.39), R Ser (0.26), W Lyr (0.94), and χ Cyg (0.04). As mentioned above, $H\alpha$ is notorious for being observed as a weak emission feature when $H\beta$, $H\gamma$, and $H\delta$ are strong. Surprisingly though, $H\alpha$ emission was not seen in various spectra where we would expect to find it: R Tau (phase 0.16 and 0.99), R Leo (0.16 and 0.25), V CVn (0.12, 0.27, and 0.06), R CVn (0.20), V Boo (0.12), and T Her (0.15).

Merrill (1940) and Joy (1926) report that the TiO bands are regularly stronger at minimum than at maximum light in Mira variables. To measure this trend, we checked the variability of the TiO feature at 7054 Å (band head) with respect to a portion of the flux uncompromised by TiO, VO,

and ZrO. We integrated the flux of each spectrum in the 695–7045 Å wavelength band (non-TiO) and the 7060–7110 Å band (TiO), each 50 Å wide. We then divided the integrated flux of the TiO band by the non-TiO band. By doing this, any scattered light that may have been in the spectra is effectively canceled out. Since our data set contains warm oxygen-rich (earlier than M6), cool oxygen-rich (M6–M8), and one MS Mira sampled sporadically over various phases, we only include the cool oxygen-rich Mira variables in Figure 2, which graphs the aforementioned flux ratio as a function of phase. The M6–M8 stars are selected here to minimize the spread of effective temperatures at maximum light, which will influence the strength of the TiO bands. Ideally, one would want many observations of each star over a single pulsation cycle. However, with the limited sample we have, we feel that we can obtain an approximate test of TiO variation with respect to phase. There appears to be no obvious trend in variations in the TiO 7054 Å band flux with respect to the non-TiO band flux. Because of this observation, variations seen in H α as a function of phase must primarily result from variations in the H α emission itself and not from variations in overlying TiO absorption. As a result, using H α flux variations as a proxy for variations in the intrinsic He flux is valid from this analysis.

4. DISCUSSION

We wish to test the idea that the apparent lack of He emission at 3970 Å, when the other Balmer lines are strong emission features, is anticorrelated with the strength of the Ca II absorption line at 8662 Å. As reported in § 1, this anticorrelation results from He photons being scattered by the Ca II H line out to the Ca II line at 8662 Å, causing this Ca II absorption line to be *filled in* with respect to the other two Ca II IR triplet lines.

We use H α as a proxy for the He line. Following the analysis presented by CL97, we determined a relative *line strength*, F , for H α emission and the Ca II IR triplet absorption lines. Two points were selected on either side of the emission or absorption feature. The wavelengths of these points were kept constant for all measurements. The observed *profile* was integrated across the wavelength window defined by these two points, resulting in an integrated flux f_i . A straight line connected between these two points represents a *pseudocontinuum*, and the integrated flux, f_c , is calculated for it. Then

$$F = (f_i - f_c)/f_c,$$

where F will be negative for absorption lines and positive for emission lines. The measurements were done for the stars in our sample, where their spectra included wavelengths below 6563 Å and above 8662 Å; a total of 27 spectra. Figure 3 shows the relative line strengths of H α and the Ca II 8498, 8542, and 8662 Å absorption lines as a function of phase. The uncertainty in the measurements is about ± 0.007 . The relative line strength of H α clearly shows a large scatter near visible maximum and is zero within the uncertainty from phase 0.5 to 0.8. This is consistent with Balmer emission lines becoming prominent near maximum visible light. The Ca II 8498 Å line strengths are zero, within the uncertainty of the measurements; variation is not observed in this line. The Ca II 8542 Å line does show some scatter near phase 0.0, and is zero after phase 0.2. The Ca II 8662 Å line shows more scatter than either of the other two Ca II IR triplet lines, particularly near phase 0.0.

From Figure 3, it is difficult to see any correlation

between the relative line strength of the H α and Ca II IR triplet lines. However, we can plot the relative line strengths of Ca II IR triplet lines versus the strength of the H α line to look for correlations. Figure 4 shows the relative line strengths of Ca II 8498, 8542, and 8662 versus the relative line strength of H α . The data of each plot are linearly fitted and the results of the fits are drawn in the plots. The slopes of the Ca II 8498 and 8542 relative line strengths versus H α are 0.08 and 0.05, respectively. The slope of the linear fit of the Ca II 8662 relative line strength versus H α relative line strength, on the other hand, is 0.32, which is significantly different than the other two Ca II IR triplet linear fits. Furthermore, the Ca II 8662 versus H α relative line strength slope is positive, so that as the strength of the H α line increases, the strength of the Ca II 8662 Å line decreases (i.e., becomes more positive) and even goes into emission. This is the effect we expect if He photons are being scattered by the Ca II H line out to the Ca II line at 8662 Å, causing the Ca II 8662 Å absorption line to be filled in with respect to the other two Ca II IR triplet lines.

5. CONCLUSION

The 6200 to 9000 Å spectra of Mira variables taken at different phases support a possible anticorrelation between H α emission and Ca II 8662 absorption as first suggested by CL97. Assuming that the He line strength variations are in phase with H α , then the apparent anticorrelation between the strength of the H α emission line and the strength of the Ca II 8662 Å line suggests that a *fluorescence* is taking place in the Ca II 8662 Å line, with He serving as the pump through the Ca II H line. This type of fluorescence is common in Mira type variables. The strong Fe I (42) lines at 4202 and 4308 Å seen in Mira variables are well-known fluoresced features; in this case, the ultraviolet Mg II h and k lines serve as the pump via an Fe I (UV3) transition (e.g., Bidelman & Herbig 1958; Willson 1976; Luttermoser 1996).

The next phase of this research program is to systematically determine T_{eff} and $\log g$ as a function of phase for the Mira variables in our sample. A detailed description of the LTE model synthetic spectra is given by Piontek & Luttermoser (2000).

M. W. C. greatly appreciates support from NSF grant AST 95-00756, which was the primary source of support for this research. The long-term observations required for this research project would not be possible without the continued commitment of the Southeastern Association for Research in Astronomy to provide the periodic observing times on a meter-class telescope at Kitt Peak. We thank Peter Mack of Astronomical Consultants and Equipment for his excellent technical expertise at the SARA Observatory. We also thank Robert Miller at Appalachian State University, who machined the spectrograph adapter so we could use the spectrograph on the DSO 0.45 m telescope. We are indebted to Marie Rinkoski, NSF-sponsored SARA REU student during the summer of 2000, who kindly calculated the phases, while reducing a new set of spectra as part of her research. We also greatly appreciate the comments of the referee of this paper, resulting in several significant improvements. In this research, we have used, and acknowledge with thanks, data from the AAVSO International Database, based on observations submitted to the AAVSO by variable star observers worldwide. This research has made use of the SIMBAD database, operated at CDS, Strasbourg, France.

REFERENCES

- Bertschinger, E., & Chevalier, R. A. 1985, *ApJ*, 299, 167
 Bidelman, W. P., & Herbig, G. H. 1958, *PASP*, 70, 451
 Bowen, G. H. 1988, *ApJ*, 329, 299
 Brown, J. A., Johnson, H. R., Alexander, D. R., Cutright, L., & Sharp, C. M. 1989, *ApJS*, 71, 623
 Castelaz, M. W., & Luttermoser, D. G. 1997, *AJ*, 114, 1584 (CL97)
 Contadakis, M. E., & Solf, J. 1981, *A&A*, 101, 241
 Crowe, K., Heaton, B., & Castelaz, M. W. 1996, *Int. Amat.-Professional Photoelectric Photom. Commun.*, No. 68, 30
 Fleischer, A. J., Gauger, A., Sedlmayr, E. 1992, *A&A*, 266, 321
 ———. 1995, *A&A*, 397, 543
 Gillet, D. 1988, *A&A*, 192, 206
 Gillet, D., Maurice, E., & Baade, D. 1983, *A&A*, 128, 384
 Gillet, D., Maurice, E., Bouchet, P., & Ferlet, R. 1985, *A&A*, 148, 155
 Haniff, C. A., Ghez, A. M., Gorham, P. W., Kulkarni, S. R., Matthews, K., & Neugebauer, G. 1992, *AJ*, 103, 1662
 Höfner, S., Jørgenson, U. G., Loidl, R., & Aringer, B. 1998, *A&A*, 340, 497
 Joy, A. H. 1926, *ApJ*, 63, 281
 ———. 1947, *ApJ*, 106, 288
 ———. 1954, *ApJS*, 1, 39
 Kurucz, R. L. 1970, *ATLAS: A Computer Program for Calculating Model Stellar Atmospheres* (SAO Spec. Rep. 309) (Cambridge: Smithsonian Astrophys. Obs.)
 Labeyrie, A., Koechlin, L., Bonneau, D., Blazit, A., & Foy, R. 1977, *ApJ*, 218, L75
 Loidl, R., Höfner, S., Jørgenson, U. G., & Aringer, B. 1999, *A&A*, 342, 531
 Luttermoser, D. G. 1996, in *ASP Conf. Ser. 109, Ninth Cambridge Workshop on Cool Stars, Stellar Systems, and the Sun*, ed. R. Pallavicini & A. K. Dupree (San Francisco: ASP), 535
 Luttermoser, D. G., & Bowen, G. H. 1992, in *ASP Conf. Ser. 26, Seventh Cambridge Workshop on Cool Stars, Stellar Systems, and the Sun*, ed. M. S. Giampapa & J. A. Bookbinder (San Francisco: ASP), 558
 Luttermoser, D. G., Bowen, G. H., & Willson, L. A. 2000, in preparation
 Maciel, W. J. 1977, *A&A*, 57, 273
 Merrill, P. W. 1940, *Spectra of Long-Period Variable Stars* (Chicago: Univ. Chicago Press)
 Pickering, E. C. 1887, *Nature*, 36, 32
 Piontek, R., & Luttermoser, D. L. 2000, *BAAS*, 31, 1238
 Turnshek, D. E., Turnshek, D. A., Graine, E. R., & Boeshaar, P. C. 1985, *An Atlas of Digital Spectra of Cool Stars* (Tucson: Western Research Corp.)
 Willson, L. A. 1976, *ApJ*, 205, 172
 ———. 2000, *ARA&A*, 38, 573
 Willson, L. A., & Hill, S. J. 1979, *ApJ*, 228, 854
 Wing, R. F. 1967, Ph.D. thesis, Univ. California, Berkeley
 Zhou, X. 1991, *A&A*, 248, 367

Note added in proof.—The method of phase determination used in this paper is not the standard method used by the AAVSO. We used the AAVSO light curves observed at the same time as our observations to determine the phases. The AAVSO standard method to derive official dates of maximum and minimum may give different phases.